Surface & Coatings Technology xxx (2012) xxx–xxx

Contents lists available at SciVerse ScienceDirect

Surface & Coatings Technology

journal homepage: www.elsevier.com/locate/surfcoat

Enhancement of amorphous phase formation in alumina–YSZ coatings deposited by suspension plasma spray process

Fariba Tarasi [a,*], Mamoun Medraj [b], Ali Dolatabadi [c], Jorg Oberste-Berghaus [d,1], Christian Moreau [d]

[a] Concordia University, Bahen Center, 40 St. George St., Room#8266, University of Toronto, Toronto, ON, Canada M5S 2E4
[b] Concordia University, S-EV 4411, 1455 de Maisonneuve Blvd. W, Montreal, Quebec, Canada H3G 1M8
[c] Concordia University, S-EV 12109, 1455 de Maisonneuve Blvd. W, Montreal, Quebec, Canada H3G 1M8
[d] National Research Council of Canada, 75 Boulevard de Mortagne, Boucherville, Quebec, Canada J4B 6Y4

ARTICLE INFO

Available online xxxx

Keywords:
Ceramic composite
Amorphous phase
Alumina–YSZ
Suspension plasma spray

ABSTRACT

In the present work on pseudo-eutectic alumina–yttria stabilized zirconia (YSZ) composite, the influence of spray parameters on amorphous phase formation during suspension plasma spray deposition is investigated. Several variables were evaluated as the most probable key factors influencing the amorphous phase formation. These variables include powder feed size, in-flight particle characteristics (temperature and velocity), spraying robot travel speed, preheating the substrate, number of deposition passes and the presence of bond coat. It was found that larger particle size, higher robot speed and substrate preheating lead to larger amounts of amorphous phase. Moreover, it is shown that particle velocity and temperature need to be reasonably low to get greater amorphous content while the presence of a bond coat has no significant influence on the amorphous phase formation. In contrast, increasing the number of deposition passes is detrimental to this phase. This work also discusses some correlations observed between the amorphous phase content and the in-flight particle characteristics and coating grain sizes.

1. Introduction

Alumina–yttria stabilized zirconia composites are among several potential alternative materials for thermal barrier applications [1,2]. Moreover, the superior properties of nano-structured materials are now well accepted [3,4]. Plasma spray processes are among the most important production processes permitting to deposit nano-crystallined layers. In these processes, spray powders pass through the plasma jet where they melt and accelerate toward the substrate. The molten droplets impact the substrate at high velocity and flatten into thin splats resulting in extremely high cooling rates during solidification leading to the formation of sub-micron grains. Injection of nano-sized powders is speculated as one way to deposit nano-crystalline coatings. However, using such small powder sizes imposes additional difficulties to the spray system as the powder flow tends to clog the injection hose and nozzle leading to inconsistent feeding of the powders in the plasma flow. Suspension plasma spray process (SPS) has been developed to circumvent this problem. The process employs a liquid carrier for injection of the solid fine powders into plasma jet. The solid particles suspended in the liquid and dispersed using an appropriate dispersants are much easier to inject into the plasma jet. Upon injection into the plasma, the suspension is atomized. Then, the liquid evaporates and the fine powders melt and accelerate toward the substrate as in conventional spray processes.

During coating buildup with such high cooling rate processes, in addition to nano-crystallinity, formation of amorphous phases is highly probable. The presence of amorphous phases is another noticeable feature of thermal spray coatings. The amorphous phase formation is more likely when the spray material involves several components such as in the present composite material i.e., alumina–YSZ. Indeed, during rapid cooling, a larger variety of atoms results in more difficulties for each atom to move in its crystalline site due to interference of other types of atoms. Therefore, in thermal spraying of alumina–YSZ composites, amorphous phases mostly accompany nano-crystalline structures [5–8]. These phases, in turn, were found to be a source of nano-crystallinity upon heating [4,9,10]. In addition, in alumina–YSZ composites, the amorphous phases have transformed into nano-crystalline structure that withstands high temperatures (1200 °C) with saturation of the grain size within the range of a few tens of nanometer [5,11].

Further investigation of the roles of the amorphous phase [12,13] requires to enable producing coatings with different contents of this phase. Although amorphous phase formation in the composite coatings has been already reported in the literature, the influence of

* Corresponding author at: 40 St. George St., Room#8266, Toronto, ON, Canada M5S 2E4. Tel.: +1 416 978 0489, +1 647 858 3734.
E-mail addresses: Fariba.tarasi@utoronto.ca (F. Tarasi), mmedraj@encs.concordia.ca (M. Medraj), dolat@encs.concordia.ca (A. Dolatabadi), jorg.oberste-berghaus@bekaert.com (J. Oberste-Berghaus), Christian.Moreau@cnrc-nrc.gc.ca (C. Moreau).
[1] Current address: Bekaert Advanced Coatings NV, E3-Laan 75-79, BE-9800 Deinze—Belgium.

0257-8972/$ – see front matter © 2012 Elsevier B.V. All rights reserved.
http://dx.doi.org/10.1016/j.surfcoat.2012.10.054

spray parameters on the quantity of amorphous phases formed during spraying has barely been the focus of investigation.

While in conventional plasma spray process, some efforts has been taken to produce fully amorphous structures of alumina–YSZ composite by the help of quenching to enhance the metastable phase formation [14], this current work aims at characterizing the inherent potential of the SPS process to produce high amorphous phase content within the as-sprayed coatings. Coating samples are deposited using SPS process under various spray conditions and the role of each spray parameter on the amount of amorphous phase in the coating is investigated. Moreover, some correlation between the amorphous phase content and the coating crystallite sizes with the in-flight particle velocity are studied. These investigations aim at clarifying the importance of the cooling rate upon deposition as well as verifying the previously suggested importance of the in-flight dwelling time on the formation of amorphous phases as compared with the particle temperature [15].

2. Experimental

To find ways to vary the amount of the amorphous phase within the composite alumina–YSZ coatings deposited by SPS, a group of most probably effective variables were selected. These variables are the in-flight particle velocity and temperature, feed powder size, substrate preheating, travel speed of the spray robot, number of deposition passes and bond coat (presence and absence). These parameters seemed to be influential on the amorphous content, based on the process nature and the pre-assessment of the variables.

2.1. Spray equipment and conditions

The coating samples were deposited on mild steel substrates of 2.5×2.5 cm^2 with 0.05 cm thickness. The liquid suspension was fed from a gas pressurized reservoir toward the injection nozzle. This nozzle was incorporated in the center of the Mettech Axial III plasma torch (Northwest Mettech Corp., North Vancouver, Canada) that allows the axial injection of the suspension into the plasma jet. The plasma torch consists of three anodes and three cathodes operating on three power supplies (total power ranges from 50 to 150 kW). A 3/8″ (9.5 mm) plasma nozzle size was used and the spray distance for all samples was 50 mm. The feed rate of the spray suspensions was 1.8 kg/h.

A cooling procedure was used to prevent overheating of the substrate during spraying. This was necessary because of the short spray distance used in this study. The elements of the cooling system included an air jet impinging on the front surface of the samples, nitrogen jet cooling the back of the samples. Inter-pass pauses were also used to limit the substrate temperature to a maximum of 600 °C. During spraying, the in-flight particle temperature and velocity were measured at the spray distance using the AccuraSpray G2 (Tecnar Automation, St. Bruno, Canada).

To collect the in-flight particles, the injected suspension feed was sprayed into a large water vessel (instead of deposition on a substrate). The powders were next air dried and their micrographic pictures were provided in back scattered mode using a high-resolution field emission scanning electron microscope.

2.2. Sample preparation

In this work, samples from three sets of experiments were used. Details on the materials and sample preparation for each set are summarized in Table 1 and explained as follows.

The first set of samples was to compare the different feed particle sizes and to find the role of the spray robot speed on the amount of amorphous phase in the coating. In addition, coatings prepared for evaluation of the role of particle velocity were mostly selected from this group as explained later. Spray variables for this group are listed in Table 1 in rows number 1 to 6.

Powders used in this part were a mixture of micron-size, 13 wt.% YSZ (Unitec Ceramics, Stanford, England) nominal size 1 μm, combined with the proportional amount of 5 wt.% YSZ (Tosoh TZ-3YS, Tokyo, Japan) to produce 8 wt.% YSZ and mixed with alumina powder (Malakoff, TX, USA) nominal size 1.4 μm in a weight ratio of 60 alumina/40 YSZ. The resulting mixed powder size range was about 1 to 2 μm. This mixture was next put in suspension in ethanol with a solid weight fraction of 30%. Another suspension with the same solid content was prepared using the nano-size powders, 13 wt.% YSZ (Inframat, Farmington, CT, USA) with proportional weight of 5 wt.% YSZ to produce 8 wt.% YSZ and alumina nano-powder (Nanostructured & Amorphous Materials, Houston, TX, USA) with the same alumina-to-YSZ ratio. The nano-powder mixture size was 20–60 nm. As dispersing agents, polyethylen-eimine (PEI) (MW 25,000 Alfa Aesar, Ward Hill, MA, USA) and nitric acid both with 10% concentration were used. Suspensions were lightly ball milled for more than 24 h by introducing polymer balls in the suspension container that was placed on rotating rolls (120 rpm) in order to avoid large aggregate sizes.

The second set of samples with processing conditions listed in Table 1 as numbers 7 to 10 was used to evaluate the role of preheating and in-flight particle temperature on the amorphous content. The samples were prepared in couples where one sample was preheated using a continuous 1.5 kW YAG laser to an initial temperature of 350 °C and the other sample was at room temperature when deposition started. Three different spray conditions were used

Table 1
Spray conditions (process parameters) and the resulting amorphous measurements.

Sample #	Total gas (slm), $Ar/N_2/H_2$ (slm), current (Amps)	Robot speed (m/s)	Particle size range	$T_p \pm 50$ (°C)	$V_p \pm 20$ (m/s)	Preheat (°C)	Coating thickness (μm)/passes	DSC enthalpy ± 5% (μV·s/mg)	XRD ± 2%
1	275, 65/15/20, 200	1	Nano	2783	748	–	540/70	125	40%
2	275, 65/15/20, 200	1	Micron	2831	750	–	760/70	132	45%
3	275, 65/15/20, 200	2	Nano	2755	758	–	410/70	127	41%
4	275, 65/15/20, 200	2	Micron	2783	748	–	520/70	152	64%
5	245, 75/10/15, 240	1	Micron	2810	702	–	620/70	139	43%
6	245, 75/10/15, 240	2	Micron	2822	670	–	350/70	127	62%
7	275, 65/15/20, 200	2	Nano	3064	684	350	340/50	129	44%
8	275, 65/15/20, 200	2	Nano	3064	684	No	330/50	101	41%
9	180, 45/45/10, 190	2	Nano	2830	525	350	320/50	–	57%
10	180, 45/45/10, 190	2	Nano	2830	525	No	320/50	–	52%
11	245, 75/10/15, 200	2	Nano	3430	558	350	300/50	–	39%
12	245, 75/10/15, 200	2	Nano	3430	558	No	340/50	–	32%
13	275, 65/15/20, 200	2	Micron	2750	751	–	350/150	116	45%
14	275, 65/15/20, 200	2	Micron	2733	748	–	220/100	138	55%
15	275, 65/15/20, 200	2	Micron	2730	754	–	90/50	98	40%

Please cite this article as: F. Tarasi, et al., Surf. Coat. Technol. (2012), http://dx.doi.org/10.1016/j.surfcoat.2012.10.054

to produce different particle temperatures as per the corresponding rows in Table 1.

The third set of samples (numbers 11 to 15 in Table 1) was produced to study the role of coating thickness with a larger number of deposition passes. Also, to study the role of bond coat on the resulting coatings, two kinds of substrates were prepared. One substrate was bare mild steel blasted with #54 alumina grids producing a roughness of about 3 μm. The other was steel substrate bond coated with NiCrAlY using HVOF process resulting in a roughness of 4 μm. Three couples of samples, with and without bond coat, were coated under the same spray conditions with 50, 100 and 150 passes of alumina–YSZ composite resulting in 90, 220 and 350 μm thickness, respectively.

2.3. Measurement of the amorphous phase content

Two methods were used to compare the amorphous phase content resulting from different spraying conditions. The first method is through the XRD patterns, provided by Bruker D8-Discovery diffractometer (Bruker AXS, Inc., Madison, WI, USA). The second is based on the differential scanning calorimetric (DSC) graphs produced by TG96 (SETARAM Inc., Newark, Ca, USA) machine. Description of each method follows.

2.3.1. Comparison based on XRD patterns

The X-ray patterns from the coating surface using Cu–Kα radiation and acquisition of 0.01°/s were used. In this method, the areas under the humps in the background of the XRD patterns that are characteristic of the non-crystalline structure were measured. The ratio of the hump area to the total area of the XRD pattern, including hump and sharp peak areas, was taken as representative of the amorphous content. This "amorphous index" is complementary to the "crystallinity index" which is the ratio of the crystalline peak areas to the total peak and hump areas in the coating. The amorphous index was measured within the range of 20° to 90°, unlike the other methods used for amorphous materials with comparatively small number of crystalline peaks that are measured in a small range of angles below 40° [16]. For this current measurement, the peak-fitting program GRAMS/AI from Galactic package [17] was used.

2.3.2. Comparison based on DSC graphs

The second method for comparing the amorphous contents used in this study is based on DSC graphs. The heating and cooling rates were selected as 5 °C/min. The tests were undertaken from room temperature up to the maximum temperature of 1500 °C. The application of DSC curves in amorphous phase measurement was based on the work of Keblinski et al. [18], where the area under the endothermic peak at the crystallization temperatures, known as the "crystallization peak" is employed in the calculation of the amorphous index. The curves with larger crystallization peak area represent larger amorphous content [8,19].

2.4. Grain size measurement

Grain sizes were measured based on the Scherrer's formula [20]. For these calculations, the most reliable peaks (without overlapping or with minimal overlapping) for each phase were selected as follows: planes (111) for cubic zirconia or (110) for tetragonal zirconia both at 2θ about 30°, (200) at about 68° for γ-alumina and (300) at about 46° for α-alumina phase.

The best curve fitting using the "peak fitting" function of GRAMS software [17] was used for peak measurements i.e. widths and angles. In addition, in calculation of the grain sizes, the effect of machine broadening on the peak widths was considered.

3. Results

The results of the XRD pattern calculations for amorphous index and DSC crystallization peak measurement are summarized in the last two columns of Table 1. Table 2 reports the changes of the amorphous phase between the so-called sample couples by changing each parameter. The effect of each parameter is discussed below.

3.1. Particle size of the feed materials

The micrographs of the dried micron- and nano-powder suspensions are shown in Fig. 1(a) and (b), respectively. As observed in this figure, the aggregates of nano-powder are much larger than those of micron-powder. These aggregates mostly consist of particulates of the same material (either alumina or YSZ) rather than mixed alumina–YSZ.

The in-flight particles collected in water after spraying the micron- and nano-powder suspensions are shown in Fig. 2(a) and (b), respectively.

In this figure, it is clear that the size of the in-flight particles produced with the micron-powder suspension is smaller than that of the nano-powder suspension. This means that the smaller aggregate size before spraying ended up with the smaller sprayed particles. In addition, the particles from the micron-powder suspension, Fig. 2(a), are completely round, which indicates their full melting during their passage in the plasma plume. In contrast, the in-flight particles from the nano-powder suspension, at the end of their travel in plasma, contain a large amount of unmolten or partly molten and resolidified particles, as shown in Fig. 2(b). It is worthy to note that these suspensions were sprayed under different conditions: the average temperature and velocity for the in-flight particles of the nano-powder suspension were 3140 °C and 523 m/s, while those of the micron-powder suspension were 3050 °C and 745 m/s, respectively. It was expected at the lower velocity (leading to a longer dwell time) at higher temperature for the nano-powders would yield to a substantial proportion of melting contrary to what is observed in Fig. 2(b). However, it seems that many of the nano-powder aggregates have escaped to the cold periphery of the plasma jet and were not melted.

The coatings resulting from these suspensions are shown in Fig. 3. It can be seen that in the coating produced from the nano-powder in Fig. 3(b) the lamella is thicker and more distinct black (alumina) and white (YSZ) areas are visible than what were observed in Fig. 3(a) for the micron-powder. This is the result of the larger aggregates of nano-powders, many of which are of the same material instead of being a mixture of alumina and YSZ.

3.2. Robot speed

While other parameters are constant and the resulting in-flight particle temperatures and velocities are closely comparable, Table 2 shows that decreasing the robot speed from 2 m/s to 1 m/s results in some decrease in the amount of the amorphous phase. The change ranges between a negligible amount of 2% in the case of coatings using the nano-powders to 15% for coatings from the micron-powders, based on DSC analysis. This comparison by XRD pattern calculations for nano-powder deposition shows no change in amorphous index by robot speed, but 42% decrease in amorphous content at lower robot speed for the micron-powder coatings.

3.3. Particle velocity

To provide different particle velocities, the spray conditions were changed and two couples of samples – (2,5) and (4,6) – were produced using the micron-powder suspensions with constant robot speed. It can be seen in Table 2 that increasing in-flight particle

Please cite this article as: F. Tarasi, et al., Surf. Coat. Technol. (2012), http://dx.doi.org/10.1016/j.surfcoat.2012.10.054

Table 2
Amorphous change by process parameters within the composite coating of alumina–YSZ coated by SPS process.

Varying parameter	Larger powder feed size		Higher robot speed		Higher particle velocity		Higher particle temperature		Substrate preheating			Higher number of deposition passes	
Comparison Couples	(1,2)	(3,4)	(1,3)	(2,4)	(2,5)	(4,6)	(8,10)	(10,12)	(7,8)	(9,10)	(11,12)	(13,14)	(13,15)
Change in DTA measurements	6%	20%	2%	15%	−5%	−20%	–	–	28%	–	–	−19%	18%
Change in XRD measurements	13%	56%	0%	42%	−5%	−3%	−27%	−33%	7%	10%	22%	−22%	13%

velocities with similar or close particle temperatures reduce the amount of amorphous phase in the resulting coating. With an increase of about 48 m/s in particle velocity from sample 2 to sample 5, the amorphous content is reduced by 5%. Similarly, with an increase of 78 m/s in particle velocity from sample 4 to sample 6, the amorphous phase drops by 20%. The XRD results also support this decreasing trend of amorphous phase with increased in-flight particle velocity.

3.4. Particle temperature

Using three different spray conditions, the in-flight particle temperatures were varied while the particle velocities were still comparable and other parameters were constant. The results in Table 2 show that at very high particle temperatures (more than 3000 °C) compared with melting point of the components, coatings contain a lower amorphous percentage. Indeed, the temperature increase between sample 8 ($T_p = 3064$ °C) and sample 12 ($T_p = 3430$ °C) has ended with a 27% decrease in the amount of the amorphous phase. Similarly, comparison between sample 10 ($T_p = 2830$ °C) and sample 12 ($T_p = 3430$ °C) yielded to about 33% decrease in the amorphous content.

Such a difference is visible in Fig. 4, which shows the superimposed XRD patterns of samples 10 and 12. This figure indicates that not only the amorphous hump but also the crystalline phases are affected greatly by the higher particle temperature. In sample 12, zirconia is mainly in tetragonal phase, while in sample 10, cubic zirconia is prominent. Despite the presence of the crystalline peaks in Fig. 4, the high amorphous content of more than 50% (Table 1) can be explained by very low intensity of the crystalline peaks (maximum 900 counts compared with intensity levels beyond 5000 counts in crystalline structures) that also can be noted in the same figure.

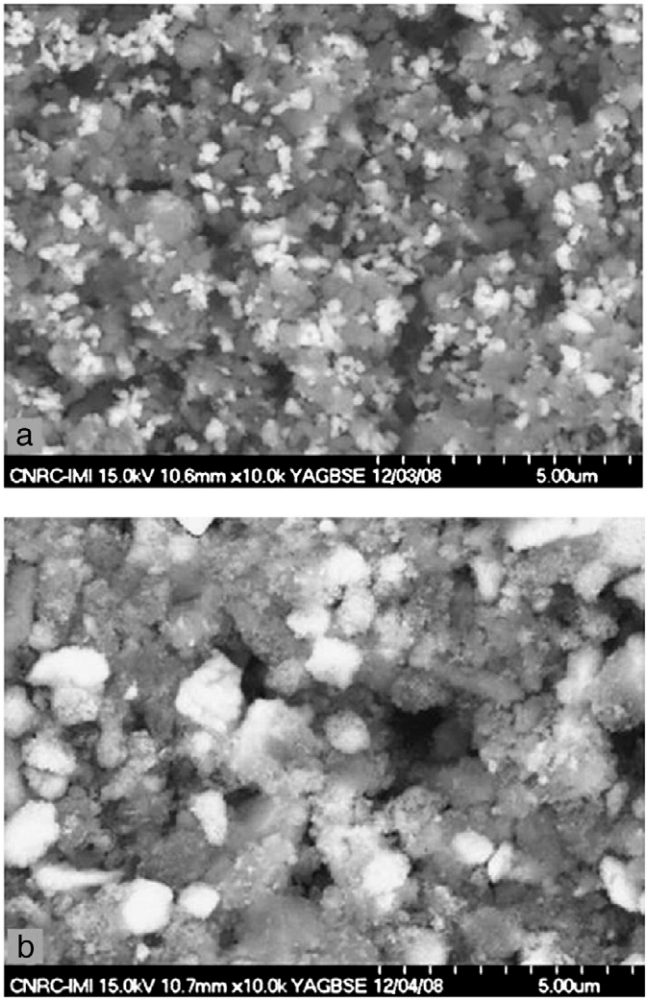

Fig. 1. SEM micrographs of aggregated powders in the suspensions showing the larger aggregates of mainly similar material (zirconia or alumina particles) formed in case of nano-size powder a) micron and b) nano-dried suspension.

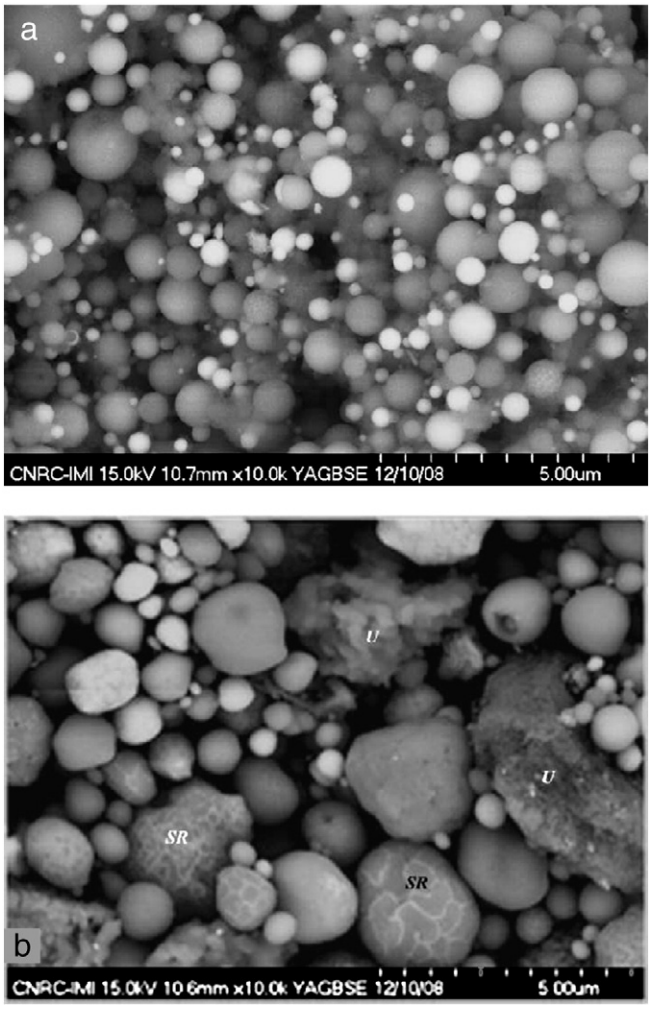

Fig. 2. Collected in-flight particles sprayed into water a) micron with fully molten round particles and b) nano-powder that contains also semi-molten and resolidified (SR), as well as unmolten (U) particles.

Please cite this article as: F. Tarasi, et al., Surf. Coat. Technol. (2012), http://dx.doi.org/10.1016/j.surfcoat.2012.10.054

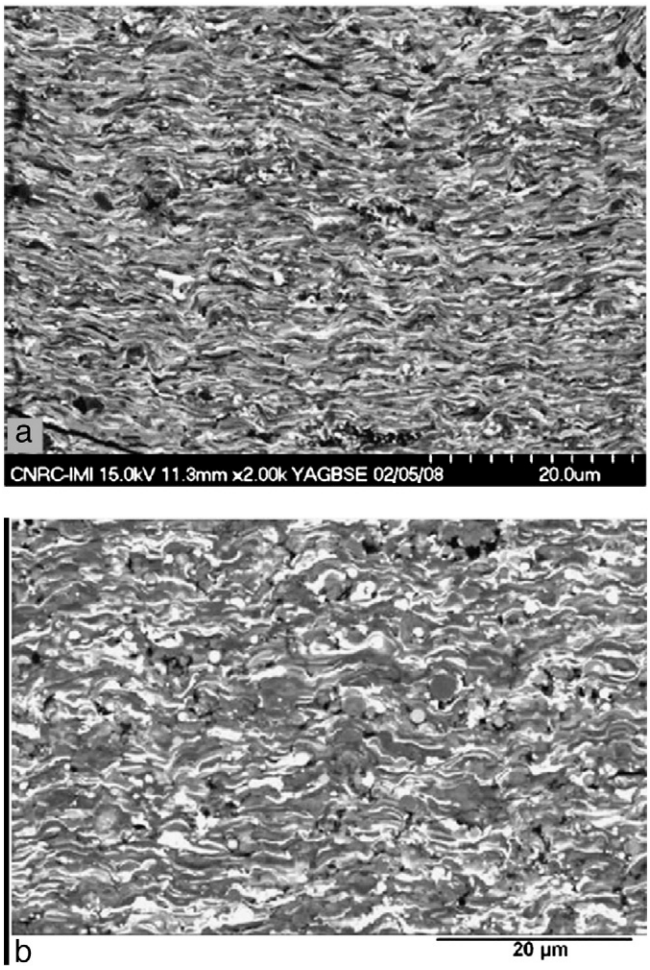

Fig. 3. Microstructures resulting from a) micron b) nano-powder deposition showing more distinct and slightly thicker lamella in nano-particle coating compared with the coating of micron particles with the same spray condition.

3.5. Substrate preheating

To study the role of the substrate preheating, comparison was first done between samples 7 and 8 by both DSC and XRD. Table 2 presents a 28% increase in DSC crystallization peak area for the coating on preheated substrate compared with the coating on non-preheated substrate. This increasing trend was confirmed by the XRD results. Two additional couples were compared just by XRD measurements in samples (9,10) and (11,12) and confirmed the above result, that is to say higher amorphous content was found in coatings deposited on a pre-heated substrate. It was also observed that preheating the substrate to 350 °C, while providing coatings of higher quality, with almost half the number of horizontal and vertical cracks, reduces the grain size of all present phases (i.e., α- and γ-alumina, t/t′ zirconia). This comparison is presented in Fig. 5. In the preheated substrate, there is normally a better interface bonding between the coating and the substrate and between the lamellae themselves [21,22]. This improved interface bonding would lead to a lower contact resistance at the interface that promotes impinging molten droplets, which results in smaller grain size in more rapid heat extraction from the all the phases formed.

It may also be noted in Fig. 5 that the grain size of the γ-alumina is smaller than in α-alumina as well as zirconia phases.

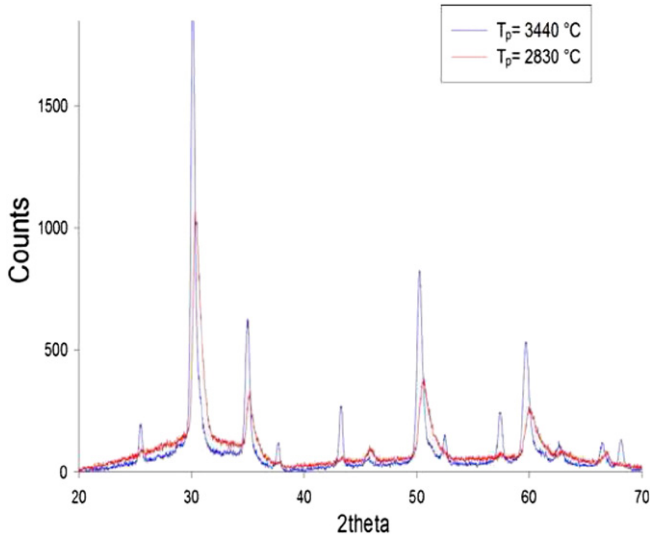

Fig. 4. XRD pattern for the two coating samples resulted from different in-flight particle temperatures showing smaller amorphous hump and higher crystallinity at higher T_p.

3.6. Number of deposition passes

Increasing the coating thickness was done by increasing the number of deposition passes under the same spray conditions. The amount of amorphous phase in the samples with 100 passes of deposition (220 µm thickness) was higher than in the coating with 150 passes (330 µm). This should be the result of increased recurrence of heating the coating to crystallization temperatures. Another reason for lower amorphous content in the thicker coating can be the reduced cooling rate because the coating acts as insulation.

3.7. Bond coat

The third set of coating samples were simultaneously deposited on mild steel bare substrates and bond coated mild steel substrates using the nano-powder suspension. The XRD patterns of the coatings on the bond coated and bare steel substrates were almost identical. This might be expected as the metallic bond coat has a thermal diffusivity close to that of the steel base material. The only difference might happen when the interface with the steel substrate to be poorer than that of bound coated substrate (as mentioned above). As long as the substrate and coating contact qualities are the same, the role of the bond coat on cooling rate, crystalline phases and even amorphous phase content should be negligible as observed here.

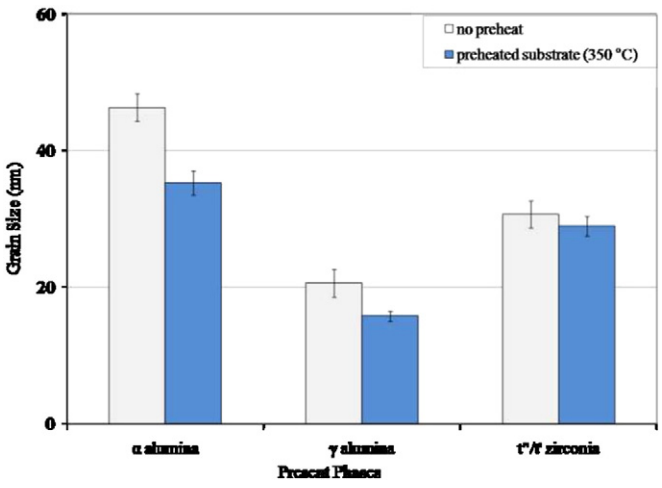

Fig. 5. Substrate preheat effect on the grain size of as deposited coating.

3.8. Amorphous content and crystallite size

The grain size of solidifying crystals depends on the cooling rate: smaller grain sizes under the same nucleation conditions can be translated to higher cooling rates. Hence, to evaluate the importance of the cooling rate on the amorphous phase formation, the grain sizes of a large group of samples have been measured, regardless of the reason for the change in the cooling rates. The relation between the grain sizes measured for each crystalline phase and the crystallization enthalpy (as an indicator of the amorphous content) in each investigated sample is illustrated in Fig. 6. In this figure, it can be seen that the smaller grain size of different phases (as a sign of higher cooling rate) is not concurrent with higher amorphous content.

3.9. Amorphous content and particle velocity

Fig. 7 shows the relationship between the amorphous phase content and in-flight particle velocity in a group of samples deposited with different spray conditions. This figure suggests that, in the presence of many other variables the general tendency for a large group of samples shows a reduced amorphous content when the in-flight particle velocity is increased.

4. Discussion

The above observations are further discussed here in the sequence of the results. The exceptions are the roles of the bond coat and the number of deposition passes which have been already discussed in the previous section.

4.1. Feed particle size

Based on the comparisons presented in Table 2, by changing the initial particle size from nano to a few microns (about two orders of magnitude larger), the crystallization peak area in the DSC graph has increased by 6 to 20%. This result is supported by XRD calculations as a 13% to 56% increase in the amorphous phase in the same couple (the larger increase has happened at higher robot speed). This suggests that nano-particles are more prone to maintain crystallinity. This is probably due to incomplete melting in the plasma jet as shown in Fig. 2(b). In addition, the lower mixing proportion observed in the molten or semi-molten particles that are transferred to the coating when using the nano-size powders reduces the chances of

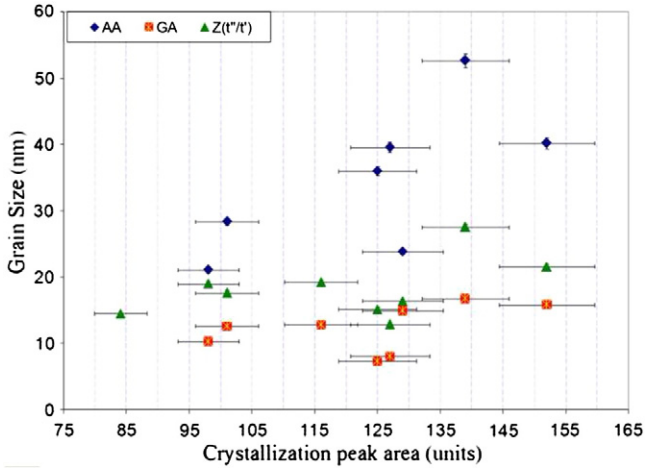

Fig. 6. Grain sizes of different phases versus crystallization peak area (as an indication of amorphous content) in each coating sample deposited under various conditions with SPS process.

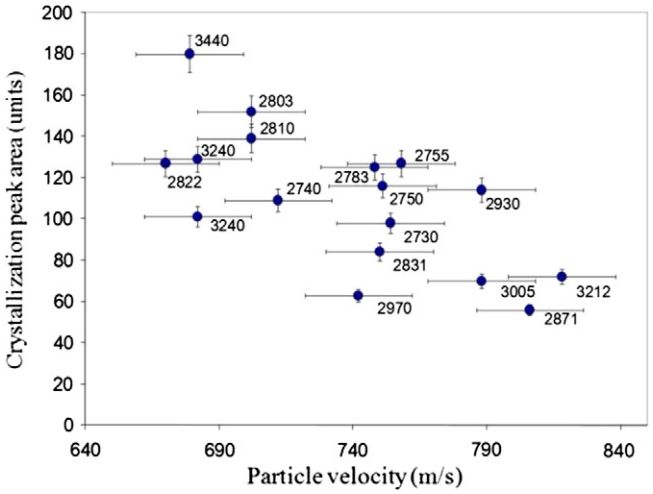

Fig. 7. Crystallization peak area vs. in-flight particle velocity showing formation of smaller amount of amorphous phase at higher velocities (The in-flight particle temperatures in °C are shown on the data points).

amorphous phase formation. The role of the in-flight alloying in this regard has been the matter of further investigation by the authors [13].

4.2. Robot speed

Considering the close distance of the torch to the substrate in SPS process compared with other common plasma spray processes, a much higher heat flux is expected to be imposed by the plasma jet to the coating during spraying [23]. Therefore, lower amorphous content at slower robot speed can be attributed to crystallization of some of the already deposited amorphous phase exposed to the high temperature plasma jet for a longer period of time. The insignificant role of robot speed in the case of nano-particle coatings is somewhat unexpected.

4.3. Particle velocity

Higher in-flight particle velocity was found to increase the formation of metastable phases such as γ-alumina and cubic zirconia due to increased cooling of the droplets upon impact on the substrate and coating top surface [24]. In a similar manner, it was expected that the amorphous phase would increase at a higher particle velocity. Thus, the observed decrease in the amorphous phase at higher particle velocities seems unexpected. This is also contrary to the reported results with pure alumina showing the amorphous phase formation concurrent with γ-alumina at the substrate interface and in extremely high cooling rate conditions [25]. Nonetheless, in alumina–yttria eutectic system the amorphous phase is reported to appear along with α-alumina [26]. This apparent conflict is investigated in further detail in Section 4.7.

4.4. Particle temperature

The increased crystallinity observed at very high particle temperature may be due to the increased reheating of the already deposited lamellae by the upcoming high temperature particles. As already noted, the temperature of the upcoming particles is far beyond the melting point of their components, but yet below their boiling point. The temperature raise of the solidified underlying splats to beyond their crystallization temperature can reduce the amorphous phase amount by crystallization process. In addition, the hot substrate promotes the formation of α-alumina at lower cooling rates [27].

Please cite this article as: F. Tarasi, et al., Surf. Coat. Technol. (2012), http://dx.doi.org/10.1016/j.surfcoat.2012.10.054

In reporting the in-flight particle temperatures in SPS process using AccuraSpray, it is noteworthy that the measurements may sometimes be influenced by the radiation emitted from the plasma jet. In such condition, the measured temperatures can be somewhat higher than they actually are. In this work, although the exact temperature measurements might be biased by the plasma radiation, its influence on relative temperature measurements from on spray condition to another one is expected to be limited making comparative measurements still possible.

4.5. Substrate preheat

This section aims at investigating the reasons for different grain sizes of the various phases formed during deposition. According to the classical theory of solidification, for heterogeneous nucleation in contact with another surface, the critical free energy for formation of each phase is given by Eq. (1) [28].

$$\Delta G_C = \frac{16\pi(\rho_l T_m)^2 \sigma^3 f_{(\beta)}}{3\Delta H_m^2 \Delta T^2} \quad (1)$$

where $\Delta T = T - T_m$ is the undercooling, σ is the solid–liquid interfacial energy, and the heat of fusion, $f_{(\beta)}$ is a function of wetting angle β. Using T_m for γ-alumina as 2289 °C and for α-alumina as 2327 °C and other data from Ref. [27], and applying the wetting angle from Ref. [29] that is below 35° for γ phase and above 45° for α-alumina, the above formula suggests that for every solidification temperature, the γ-phase has a much larger negative ΔG_c, resulting in higher nucleation rate and smaller grain sizes than the α-phase.

It should be noticed that both samples (with and without preheating the substrate at 350 °C) in this comparison are deposited simultaneously and all other parameters are exactly the same. Thus, the particles experienced the same exact melting and mixing conditions.

4.6. Amorphous content and crystallite size

Fig. 6 suggests that the cooling rate (within the range of plasma spray cooling rates) is not a dominant factor influencing the amorphous content. Actually, the amorphous content appears to be controlled by some other parameters. Fig. 6 also confirms that γ-alumina has usually the smallest grain size among the phases present, as explained above. In addition, it can be seen that there is an increase of the zirconia grain size with the amorphous phase content.

Lower amorphous content observed at higher particle velocities may be related to the in-flight mixing of the constituents after melting. Indeed, in the case of alumina and zirconia, the mixing can only occur in the molten state, since, according to their equilibrium phase diagram, they are highly insoluble in solid state [30]. In addition, the observed grain size increase in α-alumina phase at higher amounts of amorphous phase (that is coincident with lower particle velocity) can be due to the reduced cooling rate at lower particle velocities as a result of less splat flattening [23].

The difference in the extent of melting and mixing phenomena may be recognized as a fundamental characteristic of thermal spray processes in deposition of composite materials. It differentiates them from other processes involving rapid solidification. In such processes, fully molten and well mixed composite allows the comparison of the crystalline and amorphous phases simply according to the molten particle dimensions and/or the cooling rates [31].

4.7. Amorphous content and particle velocity

The time of flight and exposure to the heat of the plasma jet is controlled by the particle velocity. As mentioned previously in Section 3.9, Fig. 7 suggests that the general trend of the amorphous phase formation is reduced by shorter time of flight. Indeed, when the particle velocity is higher, the time available for the mixing of the liquid alumina and zirconia is shorter. Consequently, the amount of amorphous phase in the coatings is reduced. Such trend agrees with the previously observed results and the suggested importance of the melting and mixing processes on the coating amorphous content [15].

5. Conclusions

In this work, the roles of several parameters on the amount of amorphous phase formed within SPS coatings of alumina–YSZ composite have been studied. Larger powder feeds within the range of a few micron size are more prone to form amorphous phase than nano-sized powders. Other ways to enhance the amorphous content in spray coatings include application of higher robot speed and deposition on preheated substrate. Lower in-flight particle velocities and lower temperatures (still above the melting temperatures of the components) are also in favor of larger amorphous contents. In contrast, a larger number of deposition passes can result in a reduction of this phase in the spray coatings. Moreover, the application of bond coat has no influence on the amorphous phase formation. However, any factor that can effectively reduce the coating–substrate bonding and efficient heat dissipation from the coating can strongly diminish the formation of amorphous phase. Within the range of cooling rates encountered in the SPS process, this factor does not play a significant role on the grain size of the different phases in the deposited coatings. There is, however, differences in the grain size of the different phases in as-sprayed coatings.

In plasma spray deposition of the small composite powders using SPS process, the role of lower in-flight particle velocity surpasses the importance of higher cooling rate in amorphous phase formation. The reason most probably is related to the importance of mixing process that is a prerequisite for amorphous formation and the fact that large amount of amorphous phases in the pure materials is highly unlikely.

References

[1] P. Ramu, C.G. Saravanan, Energy Fuel 23 (2009) 653.
[2] A. Portinha, V. Teixeira, A. Monteiro, M.F. Costa, N. Lima, J. Martins, D. Martinez, Surf. Interface Anal. 35 (2003) 723.
[3] M.A. Golozar, J. Mostaghimi, T.W. Coyle, R. Soltani, in: Materials Degradation: Innovation, Inspection, Control and Rehabilitation, Proceedings of the International Symposium on Materials Degradation: Innovation, Inspection, Control and Rehabilitation, 2005, p. 273.
[4] H. Chen, X. Zhou, C. Ding, J. Eur. Ceram. Soc. 23 (2003) 1449.
[5] M. Suzuki, S. Sodeoka, T. Inoue, Trans. Mater. Res. Soc. Jpn. 29 (2004) 405.
[6] M. Suzuki, T. Inoue, S. Sodeoka, Adv. Sci. Technol. (2003) 381.
[7] H.J. Kim, K.M. Lim, B.G. Seong, C.G. Park, J. Mater. Sci. 36 (1) (2001) 49 (36, 49–54 (2001)).
[8] H.-J. Kim, Y.J. Kim, J. Mater. Sci. 34 (1999) 29.
[9] B.L. Kirsch, A.E. Riley, A.F. Gross, S.H. Tolbert, Langmuir 20 (2004) 11247.
[10] S. Sodeoka, M. Suzuki, T. Inoue, Key Eng. Mater. 317–318 (2006) 513.
[11] T. Chraska, K. Neufussa, J. Dubskya, P. Ctibora, P. Rohan, Ceram. Int. 34 (2008) 1229.
[12] F. Tarasi, M. Medraj, A. Dolatabadi, J. Oberste-Berghaus, C. Moreau, Adv. Funct. Mater. 21 (21) (2011) 4143.
[13] F. Tarasi, M. Medraj, A. Dolatabadi, J. Oberste-Berghaus, C. Moreau, J. Am. Ceram. Soc. (JUN 13 2012), http://dx.doi.org/10.1111/j.1551-2916.2012.05292.x (Article first published online).
[14] S. Dosta, I.G. Cano, J.R. Miguel, J.M. Guilemany, J. Therm. Spray Tech. 17 (2008) 360.
[15] F. Tarasi, M. Medraj, A. Dolatabadi, J. Oberste-Berghaus, C. Moreau, J. Eur. Ceram. Soc. 31 (2011) 2903.
[16] A. Lopez-Rubio, B.M. Flangan, E.P. Gilbert, M.J. Gidley, Biopolymers 89 (9) (2008) 761.
[17] November 2002.
[18] P. Keblinski, S.R. Phillpot, D. Wolf, H. Gleiter, Nanostruct. Mater. 9 (1997) 651.
[19] A. Gombas, P. Szabo-Revesz, M. Kata, G. Regdon Jr., I. Eros, J. Therm. Anal. Calorim. 68 (2002) 503.
[20] B.D. Cullity, in: Elements of X-ray Diffraction, Addison-Wesley publishing Inc., USA, California, 1978, p. 285.
[21] J. Fazilleau, C. Delbos, M. Violier, J.-F. Coudert, P. Fauchais, L. Bianchi, K. Wittmann-Teneze, in: , 2003, p. 889.

Please cite this article as: F. Tarasi, et al., Surf. Coat. Technol. (2012), http://dx.doi.org/10.1016/j.surfcoat.2012.10.054

[22] A. McDonald, C. Moreau, S. Chandra, Int. J. Heat Mass Transfer 50 (9–10) (2007) 1737.
[23] P. Fauchais, V. Rat, C. Delbos, J.F. Coudert, T. Chartier, L. Bianchi, IEEE Trans. Plasma Sci. 33 (2005) 920.
[24] F. Tarasi, M. Medraj, A. Dolatabadi, J. Oberste-Berghaus, C. Moreau, J. Therm. Spray Technol. 19 (4) (2010) 787.
[25] C. Bartuli, L. Bertamini, S. Matera, S. Sturlese, Mater. Sci. Eng. A 199 (1995) 229.
[26] M. Suzuki, S. Sodeoka, T. Inoue, in: Thermal Spray 2003: Advancing the Science and Applying the Technology, 2003, p. 701.
[27] A. Vardelle, C. Robert, G.X. Wang, S. Sampath, in: Thermal Spray, 1997, p. 635.
[28] J.W. Christian, The Theory of Transformations in Metals and Alloys, Pergamon, Elsevier Science Ltd, Oxford, UK, 2002.
[29] C. Robert, A. Denoirjean, A. Vardelle, G.-X. Wang, S. Sampath, in: Proceedings of the 15th international thermal spray conferences1998, 1998, p. 407.
[30] V. Jayarama, C.G. Levia, T. Whitneya, R. Mehrabiana, Mater. Sci. Eng. A 124 (1990) 65.
[31] Y.S.T. Ando, J. Am. Ceram. Soc. 74 (1991) 410.

Please cite this article as: F. Tarasi, et al., Surf. Coat. Technol. (2012), http://dx.doi.org/10.1016/j.surfcoat.2012.10.054